The Autotrack System

By J. S. COOK and R. LOWELL

(Manuscript received February 25, 1963)

The autotrack system accurately senses the direction of arrival, at the horn-reflector antenna, of the microwave beacon signal from the communications satellite. When this direction does not coincide with the horn-reflector pointing direction, error correcting voltages are automatically generated to enable the antenna direction system to steer the antenna toward the satellite.

This paper presents a simple analysis of error voltage generation, a description of the system, and a brief discussion of system performance. Measurements at Andover, Maine, have shown that an angular pointing error of less than 0.005 degree is maintained by the antenna when using the autotrack system to follow the Telstar communications satellite.

I. GENERAL

The autotrack system (originally designated and often referred to as the "vernier autotrack," or "VAT") is a pointing-error sensing and processing system for the horn-reflector antenna. It receives the circularly polarized 4080-mc CW beacon signal entering the antenna from the satellite, and, by examining the nature of the propagation of this signal through the antenna feed line, determines the discrepancy between the direction the antenna is pointing and the actual direction of the satellite. This discrepancy is reduced to a set of pointing-error signals to be used by the antenna pointing system to provide either a vernier correction of the programmed antenna pointing instructions, or fully automatic tracking, as shown in the block diagram of Fig. 1.

II. PRINCIPLE OF OPERATION

2.1 *Received Tracking Signals*

As a help to understanding the principle of operation of the autotrack, it is useful to think of the conical horn-reflector antenna as consisting of a conical transition from conventional cylindrical waveguide to a

very large open-end waveguide of circular cross section, having a reflective 90° bend.

Thus, if a particular mode is excited in the feed to the horn reflector, the energy propagated appears in essentially the same modal configuration in the large open cylinder that forms the antenna aperture. Only slight distortion is brought about by the asymmetry of the parabolic reflector which comprises the 90° bend. In all essential characteristics, then, the pattern of radiation from the antenna generated by exciting a particular waveguide mode in the throat of the horn will be like that radiated from a large open-ended circular waveguide excited in the same mode. It is to be recognized that the antenna is a reciprocal device, and that its radiation characteristics hold for transmission and reception alike. Hence, nothing is lost in treating the antenna from a radiating point of view, even though the scheme here described operates on a received CW signal.

In this discussion our interest will be confined to the two lowest-order modes in cylindrical guide: namely the TE_{11}, or dominant, mode and the TM_{01} mode. In fact, the waveguide feed to the horn-reflector antenna at Andover is of such diameter as to cut off all higher modes of propagation at the beacon frequency. The field configurations of the two admitted modes are shown in Fig. 2. Solid lines depict electric fields; dotted lines, magnetic.

Chu[1] has worked out general expressions for the far-field radiation patterns for open-ended circular guides. Though the expressions neglect the discontinuity at the waveguide opening, and are therefore of questionable validity near cutoff frequency, their validity from that point of view is unquestionable for a very large waveguide diameter $\approx 280\ \lambda$.

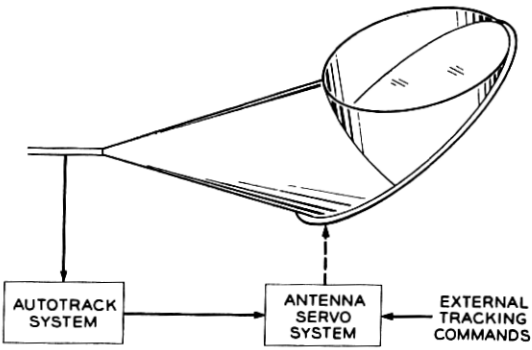

Fig. 1 — Autotrack connection with the antenna servo system.

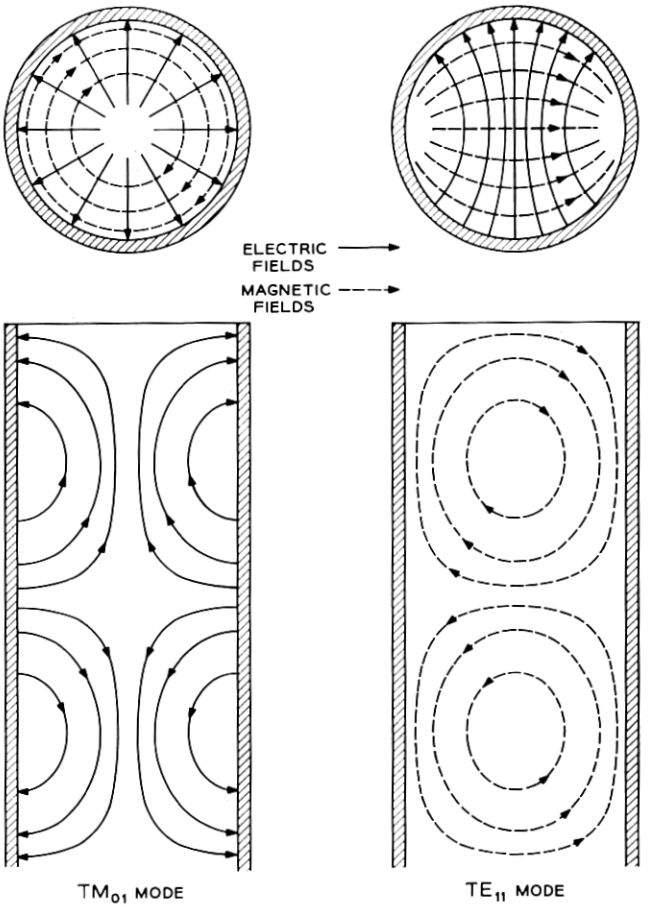

Fig. 2 — Circular waveguide mode field configurations.

The relative amplitude of the far electric fields excited by the radiation of the TM_{01} mode from a large open waveguide is:

$$E_\theta = \frac{E_0}{kR} \frac{J_0(ka\theta)}{\theta\left[\left(\frac{2.405}{ka\theta}\right)^2 - 1\right]} \qquad (1)$$

$$E_\phi = 0$$

$$E_R = 0.$$

For the vertically polarized TE_{11} mode, the far field is characterized by

$$E_\theta = \frac{E_1}{kR}\left[\frac{J_1(ka\theta)\sin\phi}{\theta}\right]$$

$$E_\phi = \frac{E_1 a}{R}\left[\frac{J_1'(ka\theta)\cos\phi}{1-\left(\frac{ka\theta}{1.84}\right)^2}\right] \qquad (2)$$

$$E_R = 0$$

where k is the free-space propagation constant, J_0 and J_1 are the zero and first-order Bessel functions, a is the waveguide (hence aperture) radius, and E_0 and E_1 are arbitrary field constants which may be rationalized in terms of the total power radiated by each mode. It turns out that $E_0 \approx E_1$. The θ, ϕ, R coordinate system is shown in Fig. 4. Both (1) and (2) assume $\theta \ll 1$; i.e., $\cos\theta \approx 1$, $\sin\theta \approx \theta$. The vertical cross sections of the patterns represented by (1) and (2) are shown in Fig. 3. The actual radiation patterns for both the TM_{01} and TE_{11}

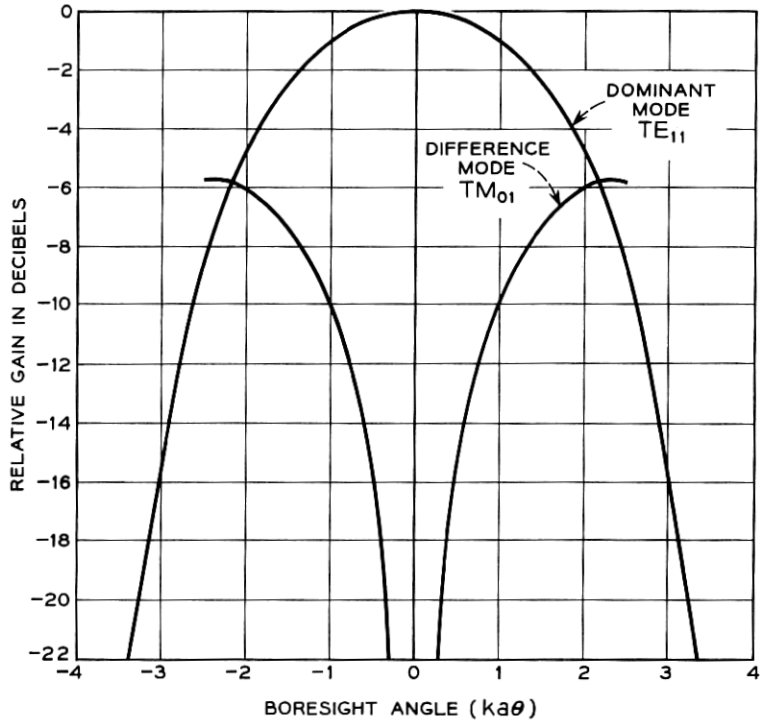

Fig. 3 — Radiation patterns for an open-end circular waveguide.

excitation of the conical horn reflector have been computed by T. G. Li and measured by J. N. Hines[2] and are, indeed, very similar to the corresponding open waveguide patterns.

The significance of the radiation patterns and their associated equations (1) and (2) becomes clear when the reciprocal condition of signal reception is considered. Fig. 4 depicts a source near the waveguide axis at the coordinate position $[\theta, \phi, R]$, where θ and ϕ describe the antenna pointing error. It is assumed that this source is, in general, elliptically polarized. The TM_{01} field-pattern shows that a TM_{01} signal will be excited only by the θ component of incident field, E_θ, and not by the ϕ component. The phase and magnitude of the TM_{01} signal at some reference point in the waveguide will therefore be determined by the phase and magnitude of the E_θ, or ϕ plane component. The magnitude of TM_{01} mode is dependent upon pointing error. For zero error, when the source lies on the waveguide axis, the pattern shows a deep null, indicating that no TM_{01} signal will be excited. However, when the source moves off

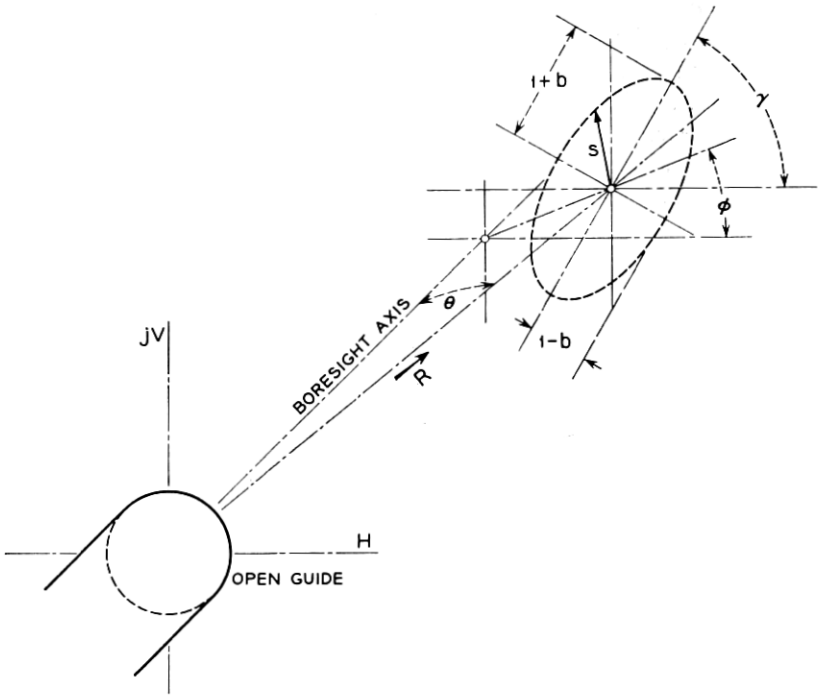

Fig. 4 — Elliptically polarized signal source and space coordinates as used in the analysis.

the waveguide axis, the TM_{01} mode will be strongly excited. When θ is small ($ka\theta < \frac{1}{2}$), (1) may be simplified to

$$\begin{aligned} E_\theta &= \frac{E_0 k a^2 \theta}{2.405R} \\ E_\phi &= 0 \\ E_R &= 0 \end{aligned} \tag{3}$$

which shows that the amplitude of the TM_{01} signal in the waveguide is directly proportional to small pointing error. It will be shown below that these characteristics, an amplitude proportional to pointing error and a phase determined by the θ component of field (that is, the component in the ϕ plane or R-θ plane), allow the TM_{01} signal to be used as an indication of the magnitude (θ) and direction (ϕ) of the pointing error.

The TE_{11} signal provides a reference against which the phase and amplitude of the TM_{01} signal are measured. Its utility for this purpose arises from two properties inherent in (2). First, the magnitude is approximately invariant with pointing error, θ, when θ is small, thus providing a magnitude reference to extract the effects of range. Second, for small θ, the TE_{11} mode is excited by both the θ and ϕ components of field in such a way that the polarization of the incoming signal is preserved; and the measurement of any two orthogonal components of the TE_{11} mode will determine this polarization. This property enables the TE_{11} signal to function as a phase reference.

The TE_{11} and TM_{01} radiation patterns resemble in form and function the "sum" and "difference" patterns, respectively, of conventional simultaneous lobing tracking systems. The conventional designations, "sum" for TE_{11} and "difference" for TM_{01}, will henceforth be used in this paper. The phase and amplitude relationships for these signals will now be derived.

2.2 *The Sum and Difference Signals*

The beacon wave expected from the satellite will be circularly polarized, though sometimes imperfectly. For generality, it will be assumed that the source, S, generates an elliptically polarized wave. Referring again to Fig. 4 for definitions of coordinates, the rotating field vector thus generated in the aperture can be simply expressed in terms of two counter rotating vectors: a positively rotating vector of amplitude, e_0/R, and a negatively rotating vector of amplitude, $b(e_0/R)$. The constant e_0 represents effective radiated power and propagation factors. The R represents range and accounts for the $1/R$ attenuation

of the wave as it radiates from the source. The two vectors rotate at an angular velocity ω. In order to permit the use of complex vector notation, the H-V plane (transverse to the guide axis) is pictured in Fig. 4 as a complex plane with the vertical axis designated as imaginary. The incident wave can then be expressed as

$$E_S = \frac{e_0}{R} (e^{j\omega t} + be^{-j\omega t}) e^{j\gamma} \tag{4}$$

where b determines the signal ellipticity, and γ determines the inclination of the major axis of the ellipse in the complex plane. As seen in the figure, the source is located at a small error angle, θ, off the open waveguide axis, and lies in a plane through the axis which is inclined an angle ϕ counterclockwise from the horizontal plane.

In the autotrack system, the horizontal and vertical components of the dominant mode are sampled and amplified separately. These two sum signals, together with the sampled difference mode, constitute the three autotrack signals derived from the elliptically polarized incident wave. As discussed above, the horizontal sum signal, e_H, responds only to the horizontally polarized component of the incident wave, the vertical sum signal, e_V, only to the vertical component, and the difference signal, e_D, only to the ϕ-plane component (E_θ).

For the sum signals, the response is invariant with small error angle, θ. If the conversion of incident field to the sampled sum signals is represented by a determinable constant, c_1, the sum-signals become

$$\begin{aligned} e_H &= c_1 \operatorname{Re} [E_s] \\ e_V &= c_1 \operatorname{Im} [E_s]. \end{aligned} \tag{5}$$

For the difference signal, the response is proportional to the ϕ-plane component of E_s, Re $[E_s e^{-j\phi}]$, and to the small error angle, θ. Thus

$$e_D = c_2 \theta \operatorname{Re} [E_s e^{-j\phi}] \tag{6}$$

where c_2 is the constant of proportionality between the incident field and the sampled difference signal.

Equations (4), (5), and (6) combine to yield

$$\begin{aligned} e_H &= \frac{c_1 e_0}{R} [\cos (wt + \gamma) + b \cos (wt - \gamma)] \\ e_V &= \frac{c_1 e_0}{R} [\sin (wt + \gamma) - b \sin (wt - \gamma)] \\ e_D &= \frac{c_2 e_0}{R} \theta [\cos (wt + \gamma - \phi) + b \cos (wt - \gamma + \phi)]. \end{aligned} \tag{7}$$

These relationships do not contain the fixed differential phase shifts in the system, which will be calibrated out.

If the polarization is indeed circular, $b = 0$, it is evident that the error, θ, and error direction, ϕ, can be extracted from (7) by a straightforward comparison of phase and amplitude between e_D and e_H or e_V. If the polarization is elliptical, these quantities cannot be precisely determined unless the polarization parameters, b and γ, are known. In practice they will not be known, but the polarization will be close to circular. The sum and difference signals will therefore be processed as if polarization were truly circular, and the anomalies introduced by ellipticity will be examined below. The analysis applies only to small error angles for which the assumptions that (a) incident polarization is preserved, and (b) the difference signal is proportional to error angle, are valid. For the 67-foot aperture of the horn-reflector antenna, this linear approximation holds to about 0.035 degree. Large-error performance will be discussed later.

2.3 *Signal Processing*

It is necessary to process the sum and difference signals (7) to produce error signals proportional to the horizontal and vertical pointing errors, ϵ_H and ϵ_V,

$$\begin{aligned} \epsilon_H &= \theta \cos \phi \\ \epsilon_V &= \theta \sin \phi. \end{aligned} \tag{8}$$

The arrangement used is shown in Fig. 5. Techniques similar to simultaneous lobing, such as used in the precision tracker,[3] are involved. Taking each horizontal or vertical coordinate separately, the difference signal is first normalized with respect to the sum signal in automatic-gain-controlled amplifiers to remove common amplitude variations, such as path loss effects. The resulting normalized difference signal is then phase-compared, or multiplied, with the normalized sum signal, and then filtered to remove RF components. The process, which requires four separate IF channels combined in a horizontal-axis pair and a vertical-axis pair, yields angle-error output voltages, E_H and E_V, represented by

$$\begin{bmatrix} E_H \\ E_V \end{bmatrix} = A \begin{bmatrix} 1 & \dfrac{4b \cos \gamma \sin \gamma}{(1+b)^2 \cos^2 \gamma + (1-b)^2 \sin^2 \gamma} \\ \dfrac{4b \cos \gamma \sin \gamma}{(1+b)^2 \sin^2 \gamma + (1-b)^2 \cos^2 \gamma} & 1 \end{bmatrix} \begin{bmatrix} \epsilon_H \\ \epsilon_V \end{bmatrix} \tag{9}$$

where A is an arbitrary gain constant.

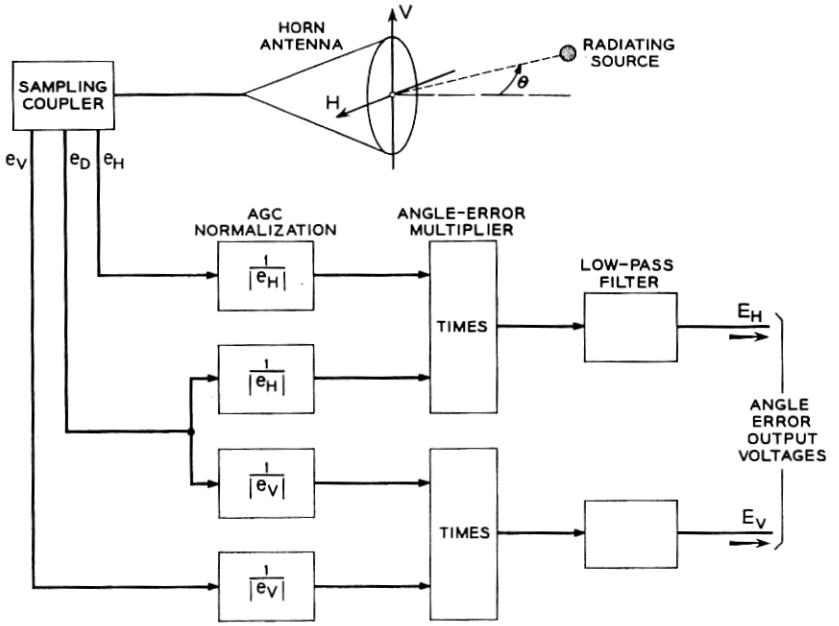

Fig. 5 — Autotrack system block diagram.

This equation shows the existence of cross coupling between the vertical and horizontal axes. The cross coupling is a function of both the ellipticity (determined by b) and the inclination of the major axis. For circular polarization ($b = 0$), the cross coupling vanishes and the error voltages become proportional to the pointing-error angles. Cross coupling also vanishes for any nonlinear polarization ($b \neq 1$) when the major axis of the ellipse coincides with the H or V axes ($\gamma = 0, \pi/2$).

The cross coupling is a consequence of the fact that, with elliptical polarization, the incident field is not a uniformly rotating, constant-amplitude vector. This is reflected in the numerator of the coupling terms, $4b \cos \gamma \sin \gamma$. The denominator results from the particular form of AGC normalization that has been used, and is not fundamental to the basic concept. The AGC system was designed to maintain constant angle-error gain in the diagonal terms of (9). Under conditions of extreme ellipticity, it magnifies the cross coupling terms when γ approaches $n\pi/2$, ($n = 0, 1, 2 \cdots$). It is therefore not the optimum technique for highly elliptical signals.

The cross-coupling coefficients of (9) vary with γ and axial ratio as shown in Fig. 6. For axial ratios less than 3 or 4 db (the maximum expected values for the Telstar satellite) the cross coupling is moderate.

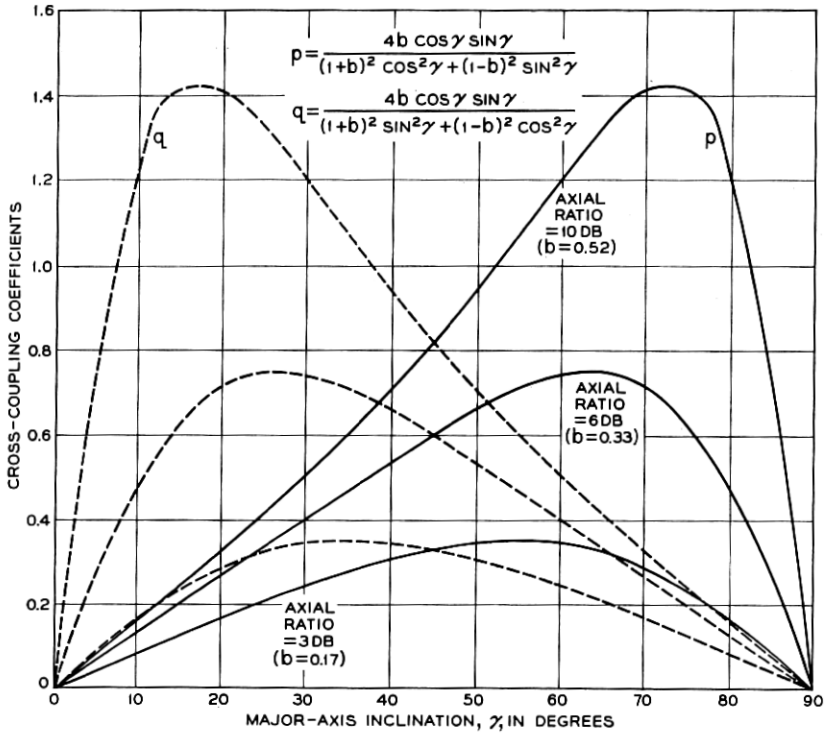

Fig. 6 — Vertical to horizontal pointing error cross coupling due to noncircular polarization of the beacon signal.

To illustrate the effects of cross coupling, (9) was used in a simple iterative error-correcting loop defined by

$$\begin{bmatrix} \epsilon_H \\ \epsilon_V \end{bmatrix}_n = [I - \delta M]^n \begin{bmatrix} \epsilon_H \\ \epsilon_V \end{bmatrix}_0 \tag{10}$$

where $[\epsilon_H , \epsilon_V]_0$ is an initial error, [M] is the error-sensing matrix of equation (9), and $[\epsilon_H , \epsilon_V]_n$ is the resulting pointing error after n iterations. The results of applying this process to two cases of different major-axis inclination and axial ratios are shown in Figs. 7 and 8. Here the arbitrary constant, δ, is chosen small enough (0.1) to plot out a smooth curve whose slope is proportional to E_V/E_H, thus illustrating the direction of the corrective influence at each point. These curves show that, in general, noncircular polarization causes correction to occur in a curvilinear path rather than in a straight line. The end-game appears to be asymptotic to

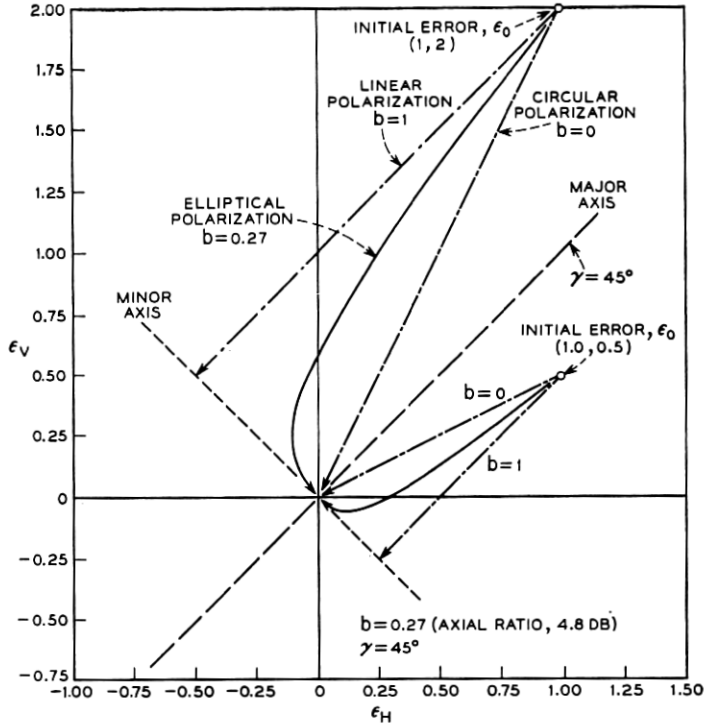

Fig. 7 — Pointing correction path of a weightless antenna in the presence of elliptic cross coupling (b = 0.27, γ = 45°).

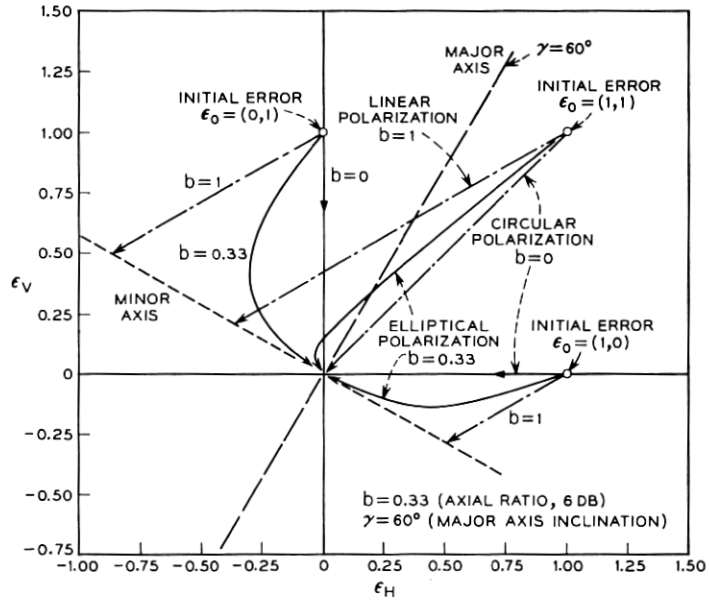

Fig. 8 — Pointing correction path of a weightless antenna in the presence of elliptic cross coupling (b = 0.33, γ = 60°).

the minor axis, implying that the coordinates could perhaps be effectively decoupled along this path. This, however, is strictly true only for $\gamma = 45°$. In general, the cross coupling must be considered in the design of a servo system. The special case of linear polarization is considered in Section 2.4.

The error correcting performance of the actual system in the full autotrack mode is shown in Fig. 9. The tracking target was the Black Mountain boresight antenna,[2] which radiates a slightly elliptically polarized signal of 2 db axial ratio ($b = 0.115$) with a major-axis inclination $\gamma \approx 10°$. A small amount of cross coupling effect is evident in these curves.

2.4 *Linear Polarization*

When the polarization is linear ($b = 1$), an error orthogonal to the plane of polarization will not excite radially symmetric electric fields in

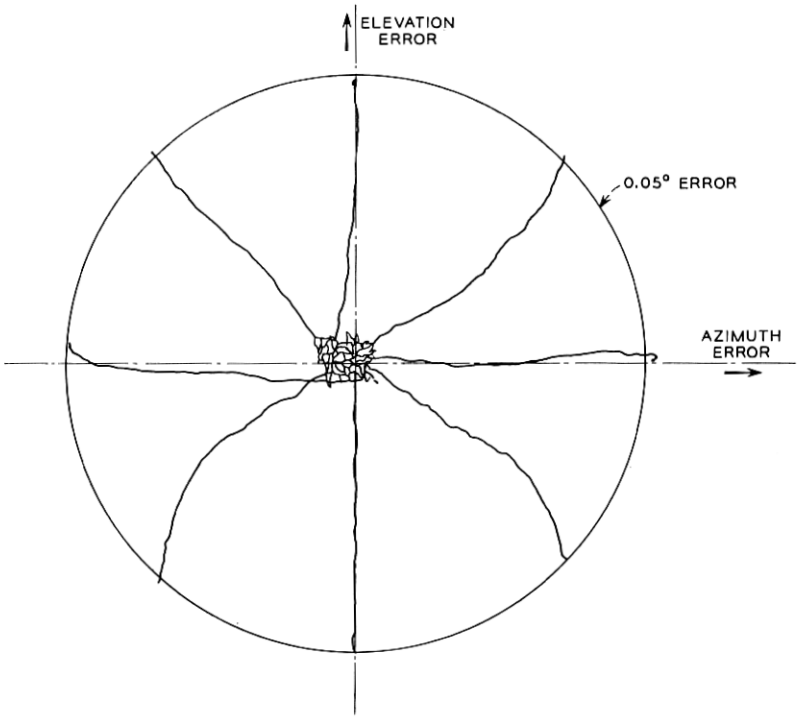

Fig. 9 — Recorded motion of the antenna, using the autotrack system to zero in on the boresight beacon.

the antenna aperture. Hence, the difference mode will not be excited, and no error indication will be generated. This may be seen from (7) and (9) by setting $\phi = \gamma + \pi/2$, to find $e_D = 0$; hence

$$\begin{bmatrix} E_H \\ E_V \end{bmatrix} = 0. \tag{11}$$

Thus, whereas for circular polarization the difference pattern has a null point on the antenna axis, for linear polarization there is a null *plane* orthogonal to the axis of polarization. Fig. 7 shows that attempts at correcting the pointing error with linear polarization result in straight-line motion terminating on the null plane. The target would then tend to slip away along this plane. Target loss of this type has been observed in tracking helicopters equipped with linearly polarized antennas. In theory, however, even a small cross-polarization component will permit full error correction, though with reduced response time.

2.5 *Two-Channel Processing*

For a satellite tracking signal that is near circular in polarization, it is possible to simplify the processing by receiving only one orthogonal component of the TE_{11} mode and generating the other with a $\pi/2$ phase shift. It is presumed here, as before, that the receiving antenna preserves polarization. Two IF channels are required, as shown in Fig. 10. The horizontal error component is obtained using the difference signal, e_D, and the horizontal sum component, e_H. The vertical error component is derived from these, as shown in the figure. The resulting error voltages are

$$\begin{bmatrix} E_H \\ \\ E_V \end{bmatrix} = A \begin{bmatrix} 1 & \dfrac{4b \sin\gamma \cos\gamma}{(1+b)^2 \cos^2\gamma + (1-b)^2 \sin^2\gamma} \\ \\ 0 & \dfrac{1-b^2}{(1+b)^2 \cos^2\gamma + (1-b)^2 \sin^2\gamma} \end{bmatrix} \begin{bmatrix} \epsilon_H \\ \\ \epsilon_V \end{bmatrix}. \tag{12}$$

For circular polarization, $b = 0$, and direct error indications without cross coupling result, as expected. For elliptical polarization with low axial ratio, cross coupling occurs, but the net effect in an error correcting loop is not much different than the four-channel scheme of (9). There is, however, one significant difference. True error sensing in the two-channel system requires prior knowledge of the sense of polarization, while in the four-channel system no prior knowledge is necessary. This may be seen by letting $b \to \infty$. A sign reversal will occur in (12) but not in (9).

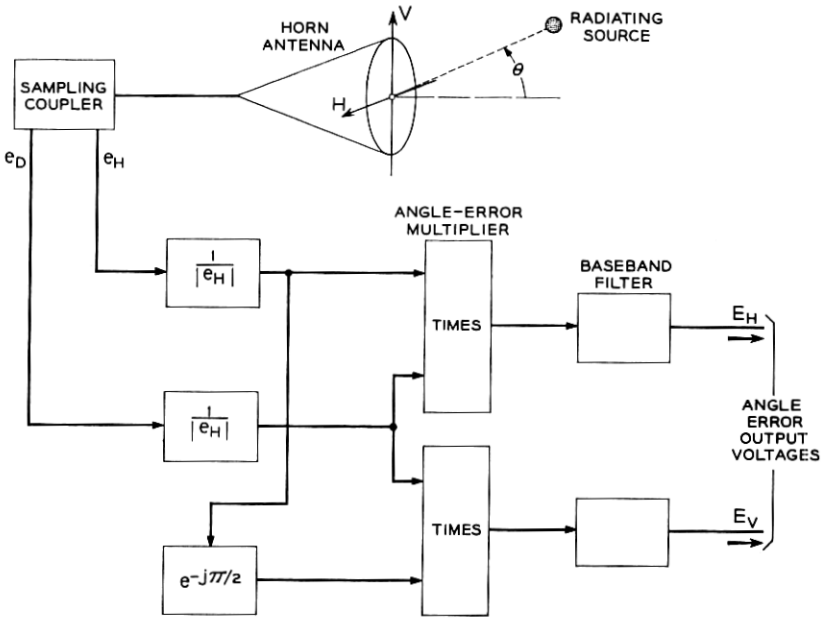

Fig. 10 — Two-channel autotrack arrangement.

The autotrack receiver was implemented for either four- or two-channel processing to permit comparison of the two techniques. The four-channel system offers some advantage in being able to handle signals of either sense of circular polarization. It also permits positive tracking on randomly polarized signals (noise). The two-channel system, on the other hand, requires less equipment.

2.6 *Large Pointing-Errors; Pull-In*

When the pointing error is large, the error voltage response is nonlinear and the receiving antenna introduces cross-polarized signals, so that the foregoing analysis is no longer valid. The resulting distortion in error-indication shows up as additional cross-coupling and effective variation in the tracking loop gain. These anomalies that accompany large error angles affect the pull-in, or angle acquisition limits, of the tracking system. Such behavior does not permit simple analysis, but experimental results show that the pull-in range is almost as large as would theoretically be obtained if circular polarization were preserved. Theoretically, the autotrack system should zero in from error angles up

to the first null in the dominant mode radiation pattern. Reliable acquisition to about 80 per cent of this angle is actually achieved. The pull-in ranges of the four-channel and two-channel systems, furthermore, are about equal.

2.7 *Coordinate Conversion*

Thus far, the analysis has been based on an open waveguide antenna in a simple H-V coordinate system lying in the aperture plane. In the actual horn-reflector antenna, the mode sampling coupler does not rotate with the horn in elevation. The error signals generated by the autotrack, designated E_x and E_y, refer to the coordinates of the mode coupler, not the aperture. The aperture-plane error signals, E_H and E_V, must be derived from these signals by a simple coordinate rotation.

Let the longitudinal and transverse (elevation) coordinates of the aperture plane be, respectively, H and V; and let the elevation angle be β. The three mode signals, referred to the aperture plane, are as given in (7). E_H and E_V are found by suitable operations on e_H, e_V, and e_D as already shown. These may be expressed in terms of transverse and longitudinally polarized modes whose coordinates are indicated in Fig. 11. Transverse fields are reversed upon reflection from the parabolic

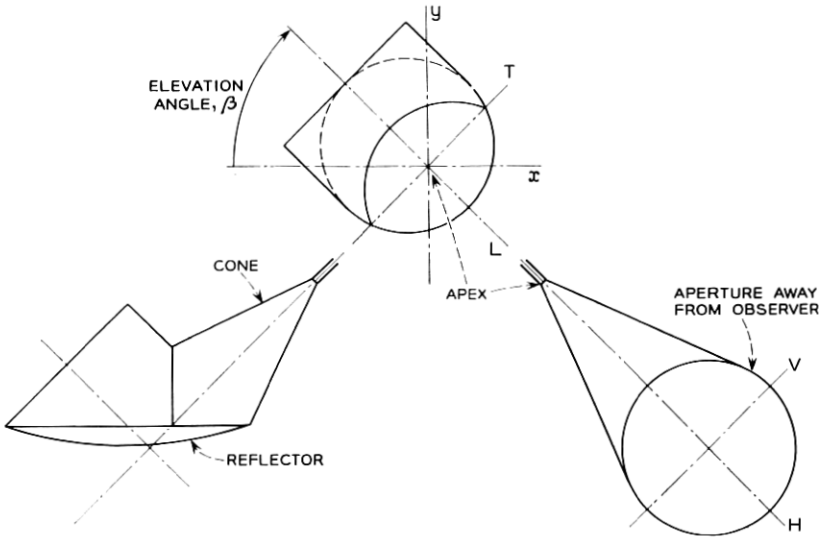

Fig. 11 — Coordinates used in determining the coordinate correction required when the horn rotates in elevation.

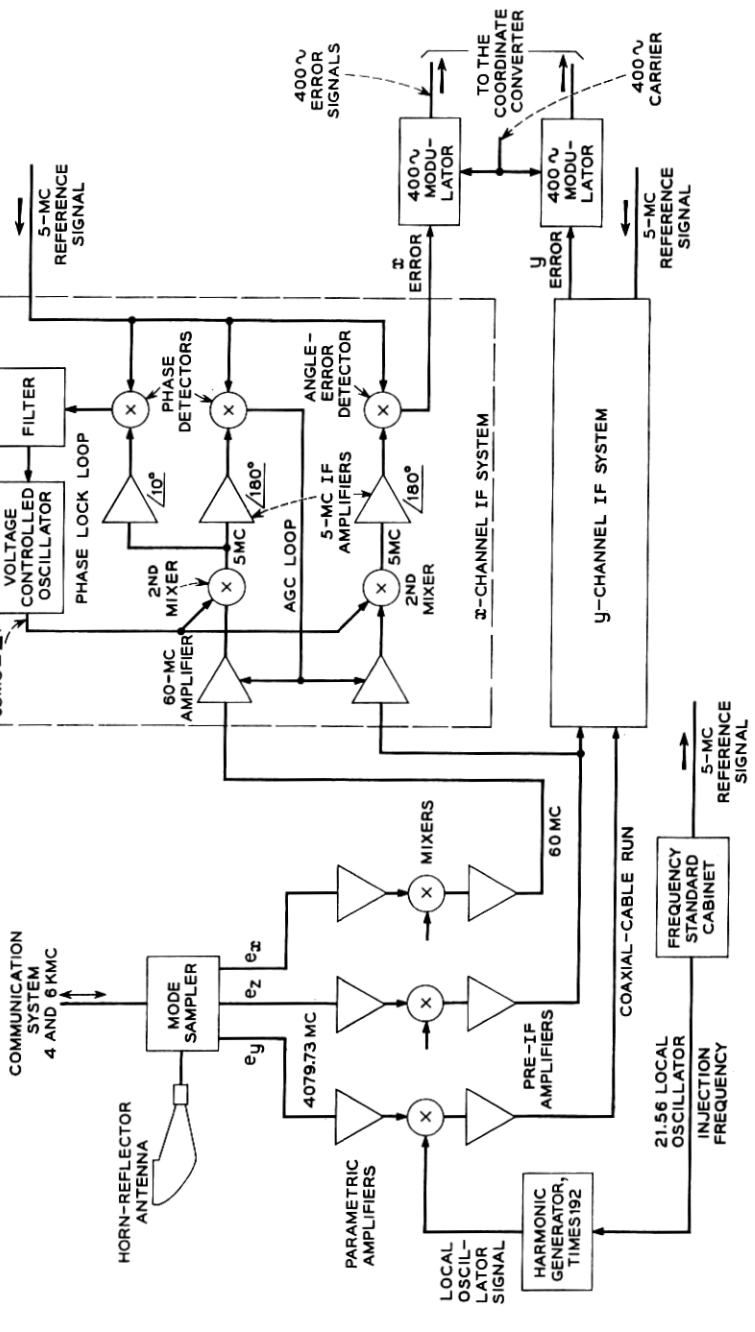

Fig. 12 — Standard four-channel autotrack system arrangement.

surface; longitudinal fields are not. Thus,

$$e_H = e_L \tag{13}$$

$$e_V = -e_T \tag{14}$$

$$e_D = -e_z \tag{15}$$

where e_z is the difference signal propagated in the z-direction.

From the figure,

$$e_L = e_x \cos \beta - e_y \sin \beta \tag{16}$$

$$-e_T = -e_x \sin \beta - e_y \cos \beta. \tag{17}$$

Then

$$e_H = e_x \cos \beta - e_y \sin \beta \tag{18}$$

$$e_V = -e_x \sin \beta - e_y \cos \beta. \tag{19}$$

Since

$$E_n = e_D e_n \tag{20}$$

equations (15), (18), (19) and (20) may now be combined to derive the required coordinate conversion. In doing this, it is necessary to invert the sign of e_x so that, for $\beta = 0$, positive x-coordinate errors will result in positive H-coordinate errors. This is done as a matter of course when the system is calibrated. The resulting transformation from error voltages referred to the mode sampler coordinates to error voltages referred to the aperture coordinates is

$$\begin{bmatrix} E_H \\ E_V \end{bmatrix} = \begin{bmatrix} \cos \beta & \sin \beta \\ -\sin \beta & \cos \beta \end{bmatrix} \begin{bmatrix} E_x \\ E_y \end{bmatrix}. \tag{21}$$

The coordinate conversion is performed on the output signals by the coordinate converter, which is part of the antenna servo system.[4] The necessity for coordinate conversion could have been avoided by rotating the coupler with the antenna in elevation. This, however, would have complicated the mechanical designs of the rotary joint and the autotrack RF circuitry.

III. SYSTEM DESCRIPTION

3.1 *General*

The block diagram of Fig. 12 shows the autotrack system hookup for four-channel signal processing. A special circular waveguide coupler

(the sampling coupler) samples the horizontal and vertical dominant modes and the difference mode excited by the 4079.73-mc beacon signal at the throat of the horn reflector. The resulting signals, e_x, e_y, and e_z, are separately amplified and down-converted in three amplifier chains. Each chain consists of a varactor parametric amplifier, a balanced mixer, and a 60-mc preamplifier. These units are located at the apex of the antenna in close proximity to the mode coupler. The three 60-mc IF signals are then transmitted, via coaxial cables, to the IF signal processing equipment located in the lower equipment room on the antenna structure. It is here that the signals are paired off for four-channel processing. Only one of these pairs, the horizontal error channel, or x channel, is depicted in detail. The other channel is identical. The signal processing for each pair consists first of IF amplification and AGC normalization in a pair of 60-mc main IF amplifiers. The signal is then down-converted to a 5-mc second intermediate frequency. At this point, the sum channel includes a phase-lock loop that works against a stable 5-mc reference signal. The phase-lock loop provides automatic Doppler tracking and permits operation with extremely weak signals. In addition, the phase coherence established by the phase-lock loop is used to advantage by performing AGC and angle-error detection coherently.[6,7] Noncoherent detection, however, is available at the turn of a switch so that the system can track on noise emitting targets such as the sun. After angle-error detection, the resulting dc horizontal and vertical angle-error signals modulate a 400-cycle carrier. They are sent to the coordinate converter in this form.

A comparison of this block diagram and that of the precision tracker[3] reveals a great functional similarity in their circuits. This fact was used to advantage to minimize the over-all development and fabrication effort. Wherever possible, the circuits and equipment were designed to be suitable for both the PT and autotrack systems. The RF and IF amplifiers, and the angle detection and frequency generation circuitry, for instance, are identical to their PT counterparts. Differences exist in the interconnection of these "building block" components to the extent that the autotrack signal processing differs from the PT processing. The autotrack also differs in (a) using dissimilar packaging of the RF "front-end" circuitry; (b) requiring a dc power supply cabinet that operates from 60-cycle, 120-volt, three-phase power; and (c) having a display and control cabinet (in place of a console) to house the 400-cycle angle modulators, status indicators, angle-error indicators, and phase-lock loop tuning controls. For circuit details of common units, the reader is referred to the precision tracker system.[3] The sampling coupler, how-

ever, is unique to the autotrack, and therefore deserves a brief description.

3.2 *Sampling Coupler*

Fig. 13 shows the autotrack RF unit in place at the apex of the horn-reflector. The sampling coupler itself is pictured in Fig. 14. Its function is to separately sample the difference mode and the vertically and horizontally polarized dominant modes excited in the antenna by the satellite microwave beacon. As an energy coupling device, the coupler is not optimum. It was designed to meet the specific needs of the satellite system, including:

(a) minimum attenuation and reflection of the 4-kmc communication signals,

(b) minimum coupling of the transmitted 6-kmc signal into the autotrack paramps, and

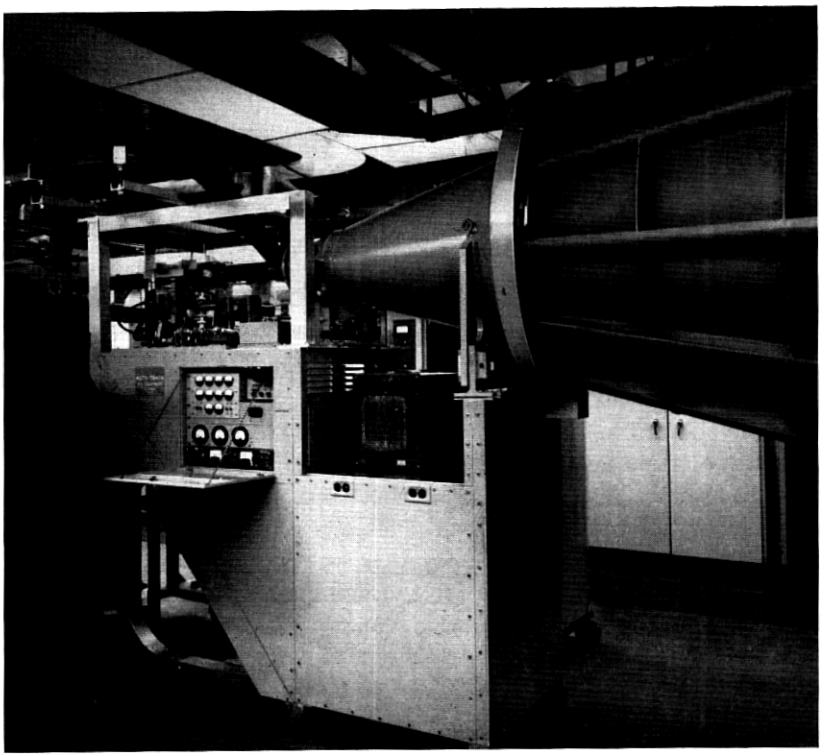

Fig. 13 — Autotrack RF unit in place at the horn apex, Andover, Maine.

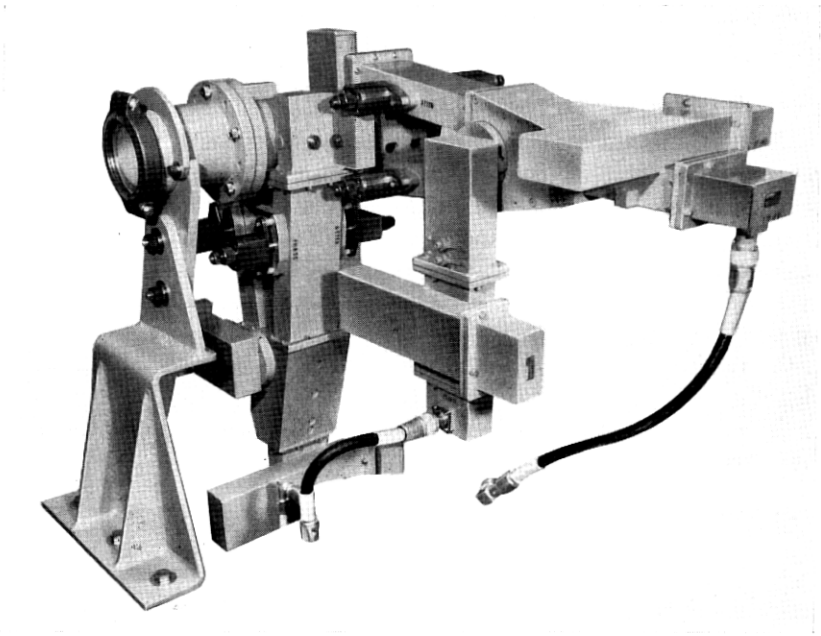

Fig. 14 — Autotrack sampling coupler.

(c) the expeditious use of existing waveguide components where possible.

The coupler takes advantage of the particular symmetry of the circular waveguide modes to separate them from one another. Fig. 2 shows that there exists a circumferential magnetic field at the cylinder walls for both types of mode — at the upper and lower surfaces for the vertically polarized dominant mode, at the side walls for the horizontally polarized mode, and all the way around for the difference mode. Because of the high gain of the large antenna, the ultimate in coupling efficiency is not necessary. It is therefore practical to magnetically couple both modes through the same holes and to separate them after coupling. The magnetic fields for the dominant modes are oppositely directed on opposite guide walls: e.g., clockwise on one side and counterclockwise on the other. By contrast, the difference mode magnetic field is continuous around the guide circumference. If balanced signals are coupled from holes on opposite sides of the guide and combined in a hybrid junction through a balanced filter and waveguide system as shown in Fig. 15, symmetry requires that energy carried by the ap-

propriate dominant mode, and that carried by the difference mode, will be separated in the hybrid.

A two-cavity filter was used to increase the coupling coefficient and provide high rejection of both transmitted and received communication signals.

Since the dominant mode components are geometrically orthogonal, they must be separately sampled using orthogonal sets of coupling holes, and they therefore require the two hybrids seen in Fig. 14. Due to the circular symmetry of the difference mode, it couples out through both sets of holes. To enhance the difference signal, the second hybrid difference arm is shorted at a point that optimizes the difference output of the first hybrid. Coupling of the difference mode is further enhanced by the fact that the waveguide at the coupler output is below cut off for that mode. The signal is reflected from the output transition, and the coupler holes are positioned to take advantage of the resulting standing wave.

The output of the coupler gives a sampling of the dominant mode beacon signal, which is about 7 db down from that received by the horn reflector; the difference mode signal is about 3 db down.

It is important to prevent coupling of the dominant modes into the tracking difference channel. This cross coupling is held about 35 db below the direct coupling level by tuning the filter cavities for a careful

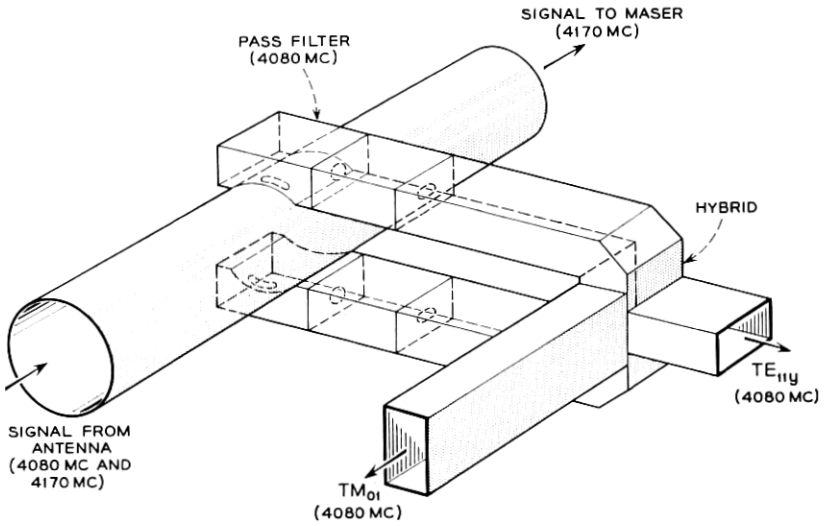

Fig. 15 — Conceptual version of the sampling coupler.

balance coincident with maximum dominant mode sampling. Additional phase and attenuation trimmers in each input arm of the hybrids provide final balance adjustment.

IV. SYSTEM PERFORMANCE

In the design of circuits for common use in both the autotrack and the precision tracker, the system gains, dynamic range, bandwidths and noise thresholds were chosen to meet the requirements of the less sensitive system, the precision tracker. Consequently, the autotrack receiver always operates well above its threshold capabilities. This threshold is determined by the ability of the phase-lock loop to remain locked in phase to the received signal despite the presence of both random phase modulation of the beacon oscillator and thermal noise. The effect of thermal noise is held to a minimum by the use of low-noise parametric amplifiers and a narrow threshold bandwidth phase-lock loop. The random phase noise is kept low by using crystal-controlled devices of high spectral purity for the satellite beacon oscillator and for the receiver beating oscillators. A practical threshold level has been experimentally determined to be about -130 dbm at the input to the sampling coupler for the horizontal and vertical dominant mode signals. Tracking accuracy is adequate for communication purposes for signals of several decibels below this value, but the angle-error gain deteriorates rapidly from its nominal value of about 100 volts/degree. The autotrack signals in normal Telstar system operation range from -90 dbm to -120 dbm.

Closed-loop tracking performance has been measured by Iwama and Norton and is discussed in more detail in their paper.[4] The acquisition angle has been found to be 0.2° in all directions, as shown by the pull-in pattern of Fig. 16. These curves show the paths taken by the antenna in zeroing in on the Black Mountain boresight antenna from an initial error angle of 0.2°. The large-angle coupling factors due to antenna-induced cross-polarization (which are not present in the small-angle pull-in patterns of Fig. 9) are evident here. These are apparent in the circumferential motion that occurs at large initial error angles, particularly in the first and fourth quadrants. The antenna motion is rather complex; it represents the combined effects of the autotrack angle-detection anomalies and the response of the servo system. The major portion of each curve is traced out in about one second.

Iwama's measurements of tracking errors show that the autotrack system maintains the null axis of the antenna within 0.005 degrees of the actual satellite direction, limited only by the tracking rate capa-

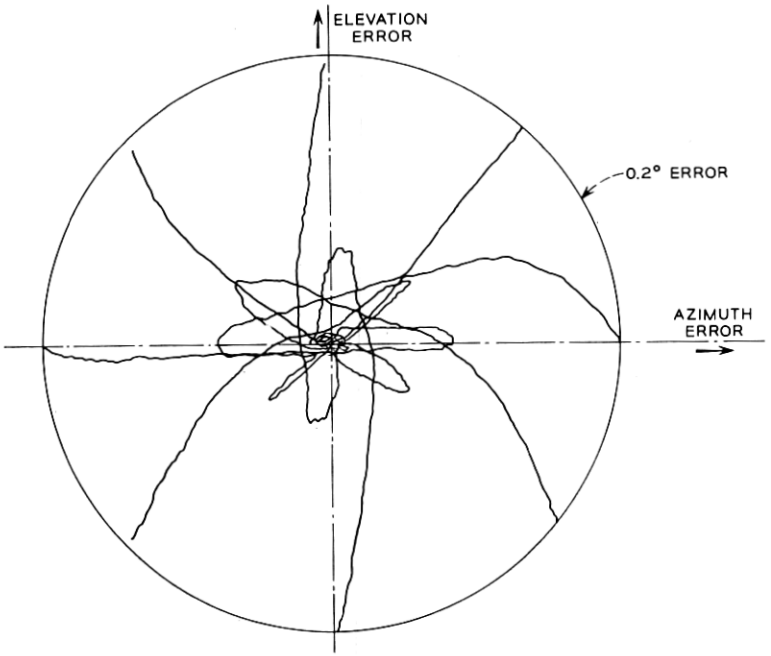

Fig. 16 — Antenna corrective motion from 0.2° initial pointing error.

bilities of the drive motors. The null axis coincides with the geometrical axis of the antenna. In the reception of circularly polarized communication signals, it is possible to obtain a small increase in gain by pointing off-axis in elevation by about 0.02°. Although it is theoretically possible to bias the error signals so as to achieve off-axis tracking by this amount, it is not done, because the gain enhancement is not significant.

The signal levels received in the autotrack system during the first Telstar communication pass are compared with predicted levels in Fig. 17. The received signal data represents points taken from a continuous recording of AGC voltage at about 0.5-minute intervals. The predicted values were based on measured satellite antenna gain patterns (shown as a smoothed curve), predicted range (also plotted), and predicted spin angle (not shown). The spread between the upper and lower predicted signal bounds, S_{MAX} and S_{MIN}, represents two factors: the ellipticity of polarization as a function of spin angle, and a variation in satellite transmitter power from 17 dbm to 19 dbm. This is the maximum power variation expected when the ground transmitter is turned on and off. As may be seen by the 2-db drop in received power at approximately 23:25

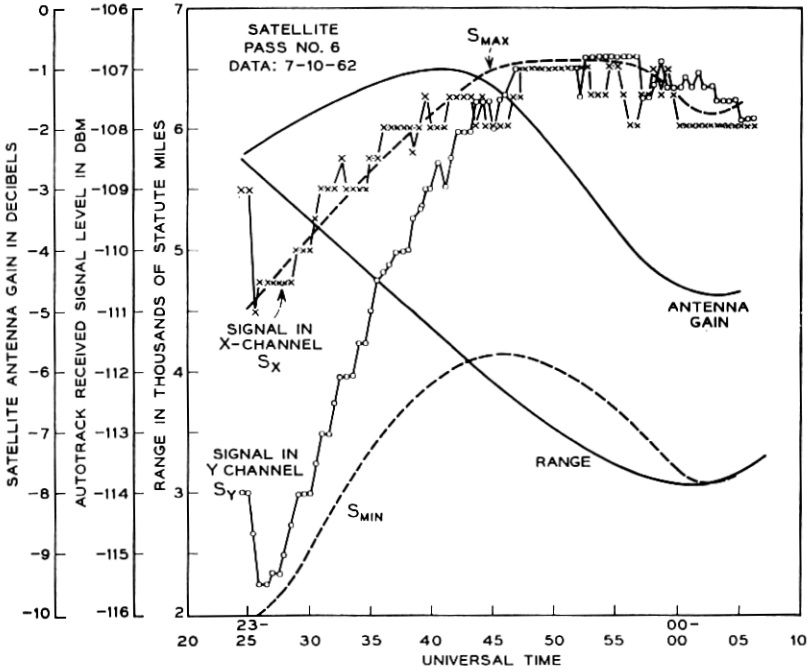

Fig. 17 — Received signal levels for Telstar satellite pass 6.

to 23:26 hours, the ground transmitter was turned on at this time and remained on for most of the pass. The 17-dbm value of satellite transmitter power should therefore have been used for prediction from that time on. Thus, after 23:26 hours, the S_{MAX} curve should have been displaced downward by 2 db in order to represent true conditions. From these considerations, it may be seen that the measured signals differed from predicted values by about +2 db. The accuracy of receiver calibration and of prediction are each about ±1 db.

The high tracking accuracy made possible by the autotrack system eliminates antenna tracking error as a limiting factor in the performance of the ground station. The basic techniques are applicable not only to the horn-reflector antenna, but also to a wide class of more conventional reflector antennas.

V. ACKNOWLEDGMENTS

The multimode sampling technique on which the autotrack system is based was jointly worked out by J. N. Hines and the authors. It was

found to be closely related to S. E. Miller's earlier work.[5] The evolution from first concept to a smoothly operating, reliable system came about through the cooperative efforts and suggestions of many, many people. We feel particularly indebted to R. V. Lohmiller and his department for detailed design and fabrication of a major portion of the equipment; to K. B. Woodard and his group for detailed mechanical design of much of the RF equipment; to E. M. Elam for final design, coordination, assembly, installation, and testing of the complete autotrack RF unit; and to E. C. Snyder, Jr. for coordinating much of the assembly, installation, calibration, testing, and operation of the autotrack system both at Andover, Maine, and Pleumeur-Bodou, France.

REFERENCES

1. Chu, L. J., Calculation of the Radiation Properties of Hollow Pipes and Horns, J. Appl. Phys., **11,** Sept., 1940, p. 603.
2. Hines, J. N., Li, T., and Turrin, R. H., The Electrical Characteristics of the Conical Horn-Reflector Antenna, B.S.T.J., this issue, p. 1187.
3. Anders, J. V., Higgins, E. F., Murray, J. L., and Schaefer, F. J., The Precision Tracker, B.S.T.J., this issue, p. 1309.
4. Lozier, J. C., Norton, J. A., and Iwama, M., The Servo System for Antenna Positioning, B.S.T.J., this issue, p. 1253.
5. Miller, S.E., Multimode Automatic Tracking Antenna System, U.S. Patent 2931033, March 29, 1960. Patent applied for July 19, 1955.
6. Nelson, W. L., Phase-Lock Loop Design for Coherent Angle-Error Detection in the *Telstar* Satellite Tracking System, to be published.
7. Ball, W. H. W., Analysis and Digital Simulation of the *Telstar* Precision Tracker, Paper No. CP-63-368, presented at the IEEE Winter General Meeting, New York, 1963.